

Theoretical investigation into the possibility of very large moments in Fe_{16}N_2

H. Sims,¹ W. H. Butler,¹ M. Richter,² K. Koepnik,² E. Şaşıoğlu,³ C. Friedrich,³ and S. Blügel³

¹Center for Materials for Information Technology (MINT) and
Department of Physics, University of Alabama, Tuscaloosa, AL 35487

²IFW Dresden e.V., P.O. Box 270116, D-01171 Dresden, Germany

³Peter Grünberg Institut and Institute for Advanced Simulation,
Forschungszentrum Jülich and JARA, 52425 Jülich, Germany

We examine the mystery of the disputed high-magnetization $\alpha''\text{-Fe}_{16}\text{N}_2$ phase, employing the Heyd-Scuseria-Ernzerhof screened hybrid functional method, perturbative many-body corrections through the GW approximation, and onsite Coulomb correlations through the GGA+U method. We present a first-principles computation of the effective on-site Coulomb interaction (Hubbard U) between localized $3d$ electrons employing the constrained random-phase approximation (cRPA), finding only somewhat stronger on-site correlations than in bcc Fe. We find that the hybrid functional method, the GW approximation, and the GGA+U method (using parameters computed from cRPA) yield an average spin moment of 2.9, 2.6 – 2.7, and 2.7 μ_B per Fe, respectively.

I. INTRODUCTION

Though discovered in 1951 by Jack,¹ $\alpha''\text{-Fe}_{16}\text{N}_2$ (with crystal structure pictured in Figure 1) first drew the attention of the magnetism community in 1972. It was then, 20 years later, that Kim and Takahashi² reported polycrystalline, mixed-phase Fe-N films with a saturation magnetization exceeding that of both $\alpha\text{-Fe}$ and $\text{Co}_{35}\text{Fe}_{65}$ ($\sim 2 \times 10^6$ A/m). However, it took another 20 years for the result to be reproduced (and, in fact, surpassed) by Sugita *et al.*^{3,4} Throughout the 1980s and '90s, other measurements of Fe_{16}N_2 thin films were reported that generally did not find this large magnetic moment.^{5–8}

Concurrently, density-functional theory (DFT) electronic structure calculations were performed,^{9–14} finding the moment per Fe ion to be modestly increased with respect to bulk bcc Fe but far short of the 3.5 μ_B reported by Sugita *et al.* It was shown¹⁵ that LSDA+U¹⁸ calculations could yield an average moment comparable to that of some experiments ($\sim 2.8\mu_B$ per Fe), but the parameters ($U \approx 3.94, 1.0, \text{ and } 1.34$ eV on the $4d, 4e,$ and $8h$ sites, respectively, with $J = U/10$) were obtained via an embedded-cluster method with a small screening constant and were not calculated from first principles. Additionally, the J parameter is smaller than usually considered appropriate for transition metals (typically one chooses either an atomic-like J of about 0.9 eV or else a more screened J of about 0.6–0.7 eV).

Recently, further experimental evidence for the large magnetization has arisen,¹⁶ as well as a companion theoretical paper¹⁷ reporting enlarged Fe moments achieved using LSDA+U (using $U = 1.0$ eV for the $4d$ site, 4.0 eV for the $4e$ and $8h$ sites, and $J = U/10$). Ji *et al.* motivate their parameters by proposing that the Fe sites in the N-Fe octahedra form strongly correlated clusters in a metallic Fe environment, choosing a small U for the (within their model) more metallic $4d$ sites and a large U (chosen to be intermediate between that of FeO and Fe) for the $4e$ and $8h$ sites. They suggest that this model is supported by XMCD spectra that show additional fea-

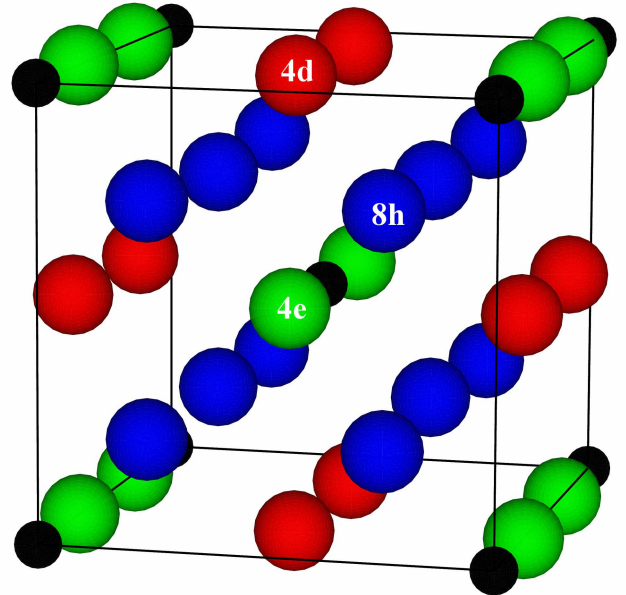


FIG. 1. (color online) Crystal structure of Fe_{16}N_2 , belonging to space group $I4/mmm$. We use the PBE-relaxed structure in all calculations with $a = 5.72$ Å, $c = 6.29$ Å, $x = 0.243$, and $z = 0.294$. We will frequently refer to the three inequivalent Fe Wyckoff sites: $4d$ (red), $4e$ (green), and $8h$ (blue) (the N sites are black).

tures at the Fe sites not seen in bcc Fe or other Fe-N phases.¹⁹

In the present work, we perform an extensive search for the proposed large magnetization; we calculate the hyperfine field at the three Fe sites and compare with published Mössbauer spectra; we search for additional energy minima at moments away from the theoretical prediction as a function of tetragonal distortion; we apply the HSE06 hybrid-functional method²⁰ and the GW approximation²¹ as implemented in VASP²² to $\alpha''\text{-Fe}_{16}\text{N}_2$, testing the two methods on bcc Fe to ensure that any enhancement of the moment we obtain is gen-

uine. Further, we compute the effective on-site Coulomb interaction (Hubbard U) between localized $3d$ electrons employing the constrained random-phase approximation (cRPA)²³⁻²⁵ (as implemented in the SPEX²⁶ extension of the FLEUR²⁷ code), allowing us to provide for the first time first-principles predictions for the U and J parameters. Finally, we present new PBE+U²⁸ calculations using these parameters and discuss their implications for existing models.

II. COMPUTATIONAL DETAILS

The hyperfine field calculation and the study of the dependence of the total energy on cell moment (fixed spin moment or FSM) and tetragonal distortion was performed using the FPL0 code.³⁰ We implemented the full relativistic expression for the hyperfine field

$$B_{HF} = \frac{\hbar^2}{ecm_e} \sum_{\nu} \left\langle \nu \left| \underline{\alpha} \cdot \left(\hat{\boldsymbol{\mu}}_n \times \frac{\mathbf{r}}{r^3} \right) \right| \nu \right\rangle \quad (1)$$

as given in Ref. 29 and references therein into FPL0³⁰. Note, that here we give the general pre-factor to accommodate for proper units. $|\nu\rangle$ are the solutions of the Kohn-Sham-Dirac equation, while $\underline{\alpha} = \begin{pmatrix} 0 & \boldsymbol{\sigma} \\ \boldsymbol{\sigma} & 0 \end{pmatrix}$, with $\boldsymbol{\sigma}$ being the vector of the Pauli matrices. $\hat{\boldsymbol{\mu}}_n$ is the direction of the nuclear spin moment. The wave functions Ψ_{ν} are expanded in local atom centered orbitals in FPL0. The effective integrand $\frac{1}{r^2}$ leads to a damping factor for matrix elements between orbitals from different sites, which allows to introduce the approximation that only terms with orbitals belonging to the atom at which the nuclear spins sits will be taken into account. The scalar relativistic hyperfine fields only contains the Fermi contact term, while the full relativistic version contains all terms (including Fermi contact, orbital and spin dipole-nuclear dipole), due to the intrinsic 4-component formulation of Eq. (1) and the use of 4-spinors. A non-relativistic limit of this expression reveals all of the separate terms. The major contributions come from the s -orbitals, for whom only the Fermi contact term contributes. Although, the core states contribute a large amount to the hyperfine field it has been shown³¹ that valence contributions can be sizable. The core contribution depends on the spin polarization of the core wave functions including the effects of the crystal exchange potential and hence should be influenced and scaled by the local spin moment. In FPL0 the semi-core (Fe 3s,3p) states are treated like valence states. For this reason we include the valence and semi-core contributions via the onsite approximation as explained above.

The FSM calculation was carried out within the PBE approximation using a $8 \times 8 \times 8$ k -point mesh in a linear tetrahedron method with Blöchl corrections. Our VASP PBE+U (using the fully-local double-counting term), HSE06 and GW calculations used a plane-wave cut-off

of 400 eV (29.4 Ry or $5.42 a_0^{-1}$). The PBE+U (HSE06 and GW) calculations used an $8 \times 8 \times 8$ ($6 \times 6 \times 6$) Γ -centered Monkhorst-Pack k mesh (also using the tetrahedron method with Blöchl corrections), employing a smaller $3 \times 3 \times 3$ mesh for the exact-exchange sums. All of our VASP calculations use the PAW³² pseudopotentials of Kresse and Joubert,³³ and all VASP moments are calculated within a sphere of radius 1.3 Å on the Fe sites.

To calculate the Hubbard U parameter we employ the constrained random-phase approximation (cRPA)²³ within the full-potential linearized augmented-plane-wave (FLAPW) method using maximally localized Wannier functions (MLWFs).^{25,34} The cRPA approach offers an efficient way to calculate the effective Coulomb interaction U and allows to determine individual Coulomb matrix elements, e.g., on-site, off-site, inter-orbital, intra-orbital, and exchange as well as their frequency dependence. We use the FLAPW method as implemented in the FLEUR code²⁷ with the PBE exchange-correlation potential²⁸ for ground-state calculations. A dense $16 \times 16 \times 16$ \mathbf{k} -point grid is used. The MLWFs are constructed with the Wannier90 code^{35,36}. The effective Coulomb potential is calculated within the recently developed cRPA method²³ implemented in the SPEX code²⁶ (for further technical details see Refs. 24, 25, and 37). We use a $3 \times 3 \times 3$ k -point grid in the cRPA calculations.

In all calculations we use the PBE-relaxed structure with $a = 5.72$ Å and $c = 6.29$ Å (except in the FSM survey) and internal parameters $x = 0.243$ and $z = 0.294$. As a final note, we consider all employed electronic structure schemes (VASP, FLEUR, FPL0) to be equivalent with respect to numerical accuracy at the level required in the present study. The use of three different packages is motivated by the different implementations available in these codes.

III. RESULTS AND DISCUSSION

A. Hyperfine Field

The hyperfine field provides a picture of the local magnetic structure that, unlike measurements of the saturation magnetization, does not require accurate estimation of the volume of a sample or its component phases. Mössbauer spectroscopy has been performed in many previous works^{3,4,8,38-41}, and the hyperfine field has been calculated^{9,12,13,42} from DFT. Our calculated B_{hf} (found along with our calculated Fe moments in Table I) agrees well with these past results; we find that the Fe sites with N nearest-neighbors exhibit approximately the same field (-23 and -22 T on the $4e$ and $8h$ sites), while $B_{hf} = -31$ T for the $4d$ sites. If we note, as previous authors have,⁹ that DFT underestimates the hyperfine field by a substantial, though nearly static, amount (~ 8 T in this case), then we also find reasonable agreement with some of the experimental reports. Particularly, we agree well with Refs. 8, 38, and 39. Although our hyperfine fields

agree numerically with those of Moriya *et al.*,³⁸ they claimed that the largest hyperfine field was to be found in the $8h$ site, a claim that is difficult to reconcile with the predicted relative magnitudes of the moments and the similar environment of the $4e$ and $8h$ sites. We note, however, that this assignment of the hyperfine fields agrees better with the moments in the recent LSDA+U study of Ji *et al.*¹⁷ We cannot offer any new explanation for Sugita *et al.*'s larger 46 T field³ nor the presence of only one Mössbauer sextet in their later single-phase sample.⁴

Site	Spin Moment (μ_B)	B_{hf} (T) (scal.-rel.)	B_{hf} (T) (rel.)
$4d$	2.85	-34	-31
$4e$	2.17	-25	-23
$8h$	2.36	-25	-22

TABLE I. Spin moments calculated within scalar-relativistic PBE and hyperfine fields (both fully- and scalar-relativistic) for each Fe site calculated within PBE using the FPL0 code.

B. Fixed Spin-Moment Survey

Generally, expansion of the lattice may not be an efficient means of increasing the magnetization of a material, as the enhancement of the spin moments may not outpace the increase in volume. However, it is known that fcc Fe, while ordinarily nonmagnetic, enters a high spin state upon expansion of the cell volume.⁴³ Therefore, we have explored the energy landscape as a function of total (spin) cell moment and $\frac{c}{a}$, allowing the former to range from 34 – 48 μ_B (corresponding to average spin moments of 2.12 – 3.0 μ_B per Fe) and the latter from 1.0 – 1.5 (holding a fixed in one set of calculations and volume fixed in another). We only constrain the total spin moment of the cell and not the magnitude of the individual moments. In principle, the moments of the three inequivalent Fe sites could be arranged in many ways to obtain the same total spin moment; however, we simply accept the converged result for each structure and total moment without seeking out other possible minima.

The results may be seen in Figure 2. We note that no additional local energy minima were observed apart from the PBE-relaxed structure ($a = 5.72$ Å, $c = 6.29$ Å, $c/a \approx 1.10$) and moment (2.44 μ_B). Although the energy minimum does tend to shift to higher moments with the increase of the volume through $\frac{c}{a}$, the enhancement is not sufficient to produce an increase in the magnetization. With a held fixed at $a_{\text{expt}} = 5.72$ Å, the average spin moment per Fe reaches 2.81 μ_B at $\frac{c}{a} = 1.5$, giving a magnetization of 1.49×10^6 A/m, compared to 1.77×10^6 A/m at the experimental $\frac{c}{a}$ and 1.75×10^6 A/m in bcc Fe. If the volume is held fixed, the average moment does not depend strongly on $\frac{c}{a}$, remaining close to the PBE value throughout and decreasing to about $2.25\mu_B$ at $\frac{c}{a} = 1.5$. This supports the standard understanding of the LSDA-

or GGA-predicted increase in the moment as arising from increased cell volume.

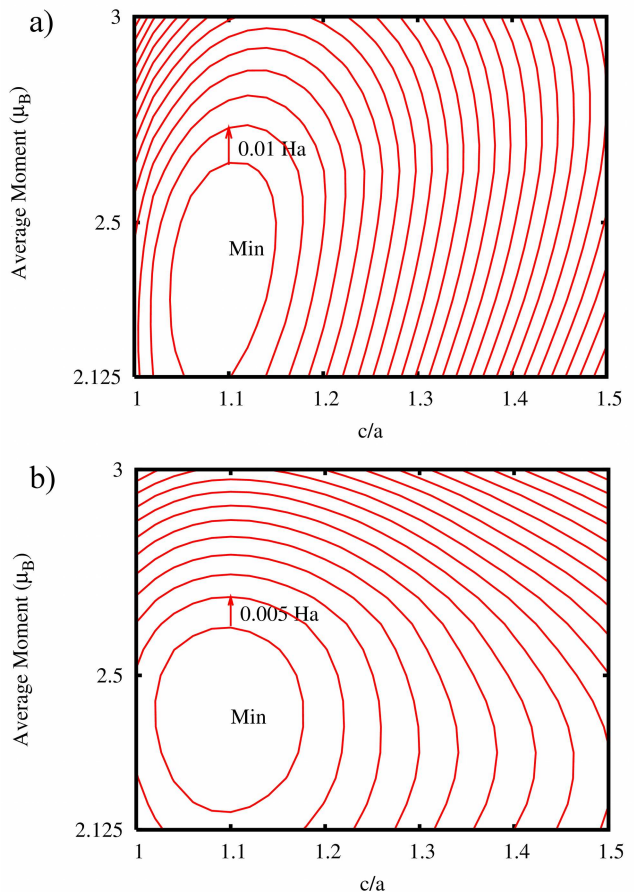


FIG. 2. (color online) Energy landscape of Fe_{16}N_2 as a function of tetragonal distortion and average moment per Fe with a) a held fixed and b) volume held fixed. Each contour represents an increase of a) 10 mHa (0.27 eV) or b) 5 mHa (0.14 eV). There are no additional local energy minima in the parameter space examined. For fixed a , $\frac{c}{a} = 1.5$ gives $\mu_{\text{avg}} = 2.81\mu_B$. Although the average moment is higher at this point, it does not overcome the increase in volume, and the magnetization is only 84% of the magnetization of the PBE structure. For fixed volume, the average moment remains close to the PBE value, decreasing slightly as c increases above $\sim 1.1a$.

C. HSE06 and GW

It is possible that DFT cannot fully account for the physics that would give rise to greatly enhanced magnetization in $\alpha''\text{-Fe}_{16}\text{N}_2$, so we have also considered methods that have arisen since the last wave of theoretical investigation into this material subsided. The HSE06 screened hybrid functional method entails only a moderate increase in computational time with respect to PBE, and the inclusion of a static screening parameter for the

exact exchange term allows for the treatment of metallic systems—unlike the parent Hartree-Fock method—as well as speeding up calculation further. HSE06 follows PBE0 in its formulation of the exchange-correlation energy, given by

$$E_{xc} = \frac{1}{4}E_x^{HF,SR} + \frac{3}{4}E_x^{PBE,SR} + E_x^{PBE,LR} + E_c^{PBE} \quad (2)$$

The aforementioned screening parameter $\mu = 0.2 \text{ \AA}^{-1}$ partitions the exchange term into a short-range and a long-range component, achieved by appending $\text{erfc}(\mu r)$ (the complementary error function) to the short-range terms and $\text{erf}(\mu r)$ to the long-range term.²⁰

The GW approximation improves upon Hartree-Fock by treating electrons as dressed quasiparticles interacting via a screened Coulomb operator W . This replaces the purely real exchange-correlation potential with a complex self energy $\Sigma = -iGW$. In the initial step, the Green's function G and the screened Coulomb operator W are calculated from the wave functions obtained from a converged DFT calculation. The computation of W via the RPA is time-consuming, and consequently some shortcuts are sometimes employed. So-called “one-shot” GW or G_0W_0 is performed by calculating the quasiparticle energies using only these initial quantities and yields improved results compared to LSDA.^{44,45} Nevertheless, the “one-shot” method still underestimates band-gaps due to the inaccuracies inherent in using an LSDA-obtained W , and improvement can be obtained by iterating G and W to self-consistency. We present results from G_0W_0 , GW_0 , and GW in this work.

Figure 3 shows the partial density of states (pDOS) of each Fe site in HSE06 and GW. For comparison, we include the PBE-calculated pDOS for Fe_{16}N_2 and a fictitious “ Fe_{16}N_0 ” structure obtained by removing the N atoms without relaxing the structure. This latter case shows that, within PBE, Fe approaches the strong ferromagnetic state, with the majority d states nearly fully occupied, upon the N-induced volume expansion, yielding an average moment of $2.56 \mu_B$ per Fe and a magnetization of $1.84 \times 10^6 \text{ A/m}$, about a 5% increase over bcc Fe (with a bulk magnetization of $1.75 \times 10^6 \text{ A/m}$). The HSE06 pDOS shows a greatly enhanced exchange splitting with respect to PBE- Fe_{16}N_0 and GW- Fe_{16}N_2 , leading to an average moment of $2.86 \mu_B$ per Fe ($M = 2.06 \times 10^6 \text{ A/m}$), whereas GW yields a more moderate $2.57\text{-}2.70 \mu_B$ per Fe ($M = 1.85\text{-}1.95 \times 10^6 \text{ A/m}$). The calculated spin moment at each site can be found in Table II.

In the absence of experimental photo- or x-ray-emission data to which to compare, we must test the validity of the calculated moments by calculating the moments of better established materials. The last column in this table shows the calculated spin moment for bcc Fe from PBE, PBE+U (which will be discussed in detail in the following section), HSE06, and GW. Our HSE06 result for bcc Fe agrees with previous work⁴⁶ and demonstrates that, although the screened hybrid func-

tional method improves on the Hartree-Fock treatment of metallic systems, it can overestimate the strength of the exchange and yield un-physical high spin states. However, we also note that the calculated bcc Fe spin moment is not necessarily directly proportional to the calculated moments in $\alpha''\text{-Fe}_{16}\text{N}_2$, so it is possible that the bcc Fe moment does not completely determine the accuracy of a method in this case.

D. cRPA and PBE+U

Previous attempts to explain the experiments that find high-magnetization have turned to LDA+U to describe the correlation effects that may be present in $\alpha''\text{-Fe}_{16}\text{N}_2$. However, as no first-principles calculations of the interaction parameters existed, it was necessary to motivate the choice of U (and J) by analogy with other systems or by applying a model. In particular, the explanation for the enhanced magnetization proposed by Ji *et al.*^{16,17} and Wang *et al.*¹⁹ requires that the Fe sites with N nearest-neighbors be more strongly-correlated than the $4d$ sites, which have no N neighbors. Without a set of firmly-established parameters, it is difficult to progress in understanding this system, as the calculated moment is directly dependent on U and J (see, e.g. Figure 3 in Ref. 17).

Recently, the cRPA has been proposed as a first-principles method of obtaining the screened Coulomb matrix within a Wannier basis.²³⁻²⁵ Within the RPA, the polarizability P can be written

$$P(\mathbf{r}, \mathbf{r}', \omega) = \sum_{\sigma} \sum_n^{\text{occ}} \sum_m^{\text{unocc}} \left[\frac{\psi_{\sigma n}^*(\mathbf{r})\psi_{\sigma m}(\mathbf{r})\psi_{\sigma m}^*(\mathbf{r}')\psi_{\sigma n}(\mathbf{r}')}{\omega - \varepsilon_{\sigma m} + \varepsilon_{\sigma n} + i\delta} - \frac{\psi_{\sigma n}(\mathbf{r})\psi_{\sigma m}^*(\mathbf{r})\psi_{\sigma m}(\mathbf{r}')\psi_{\sigma n}^*(\mathbf{r}')}{\omega + \varepsilon_{\sigma m} - \varepsilon_{\sigma n} - i\delta} \right], \quad (3)$$

where the ψ_i and ε_i are the DFT wave functions and their eigenvalues, and σ runs over both spin channels. If one separates P into P_d , containing the correlated orbitals, and P_r , containing the rest, and if one considers the unscreened Coulomb operator v , one can write^{23,25}

$$U = [1 - vP_r]^{-1}v \quad (4)$$

$$\tilde{U} = [1 - UP_d]^{-1}U \quad (5)$$

The matrix elements of the effective Coulomb potential U in the MLWF basis are given by

$$U_{\mathbf{R}n_1n_3;n_4n_2}(\omega) = \iint w_{n_1\mathbf{R}}^*(\mathbf{r})w_{n_3\mathbf{R}}(\mathbf{r})U(\mathbf{r}, \mathbf{r}'; \omega) \times w_{n_4\mathbf{R}}^*(\mathbf{r}')w_{n_2\mathbf{R}}(\mathbf{r}')d^3r d^3r', \quad (6)$$

where $w_{n\mathbf{R}}(\mathbf{r})$ is the MLWF at site \mathbf{R} with orbital index n and $U(\mathbf{r}, \mathbf{r}'; \omega)$ is calculated within the cRPA. Strictly speaking, the Wannier functions are spin dependent. However, we find that this spin dependence affects

Method	4d Site (μ_B)	4e Site (μ_B)	8h Site (μ_B)	Average (μ_B)	bcc Fe (μ_B)
PBE	2.84	2.19	2.38	2.44	2.23
PBE+U	3.08	2.62	2.74	2.71	2.67
HSE06	3.06	2.83	2.91	2.86	2.85
G ₀ W ₀	2.90	2.31	2.49	2.57	2.33
GW ₀	2.95	2.35	2.53	2.64	2.62
GW	2.96	2.41	2.57	2.66	2.65
GW (<i>s, p</i> val.)	3.00	2.50	2.64	2.70	2.59

TABLE II. Calculated spin moments for all methods presented in this work. The PBE+U results were obtained using the cRPA-obtained interaction parameters $U = 3.99, 3.12,$ and 3.52 eV for the $4d, 4e,$ and $8h$ sites, respectively ($J = 0.64, 0.59,$ and 0.61 eV), except for bcc Fe, for which we used $U = 3.16$ eV and $J = 0.68$ eV as in Ref. 25. GW (*s, p* val) denotes a VASP-GW calculation in which the Fe $3s$ and $3p$ electrons are treated on the same level as the $3d$ and $4s$.

the values only little. For simplicity, we ignore the spin dependence here and give the spin-averaged values in the following.

In our Spex-cRPA calculation, we choose the Fe d orbitals as our correlated subspace and compute the interaction parameters found in Table III. Quantities with tildes are obtained from the fully screened Coulomb matrix \tilde{U} , while plain symbols are the sp -screened quantities that enter into the PBE+U calculations. The $U, U',$ and J (and their fully-screened counterparts) are averaged at each site as follows:

$$U_{DFT+U} = F^0 = \frac{1}{25} \sum_{m,n} U_{mnmn} \quad (7a)$$

$$U = \frac{1}{5} \sum_m U_{mnmn} \quad (7b)$$

$$U' = \frac{1}{10} \sum_{m<n} U_{mnmn} \quad (7c)$$

$$J = \frac{1}{10} \sum_{m<n} U_{mnmn} \quad (7d)$$

Site	U_{DFT+U}	U	U'	J	\tilde{U}	\tilde{U}'	\tilde{J}
4d	3.99	5.02	3.74	0.64	1.80	0.71	0.53
4e	3.12	4.14	2.95	0.59	1.56	0.55	0.49
8h	3.52	4.50	3.27	0.61	1.68	0.62	0.51

TABLE III. The calculated on-site interaction parameters (all in eV) from cRPA for α'' -Fe₁₆N₂, showing a small increase in correlation with respect to bcc Fe. Quantities with a tilde are computed from the fully-screened Coulomb potential, while plain quantities are computed from the partially screened potential (omitting $d-d$ screening). U_{DFT+U} is the U parameter that enters into the PBE+U calculations.

We note that these parameters differ both quantitatively and qualitatively from previously proposed models, particularly those that suggest large differences in correlation strength between Fe sites. The spin moments from PBE+U, for Fe₁₆N₂ as well as bcc Fe, can be found in Table II. The PBE+U spin moment for bcc Fe was calculated using the interaction parameters computed in

Ref. 25— $U = 3.16$ eV and $J = 0.68$ eV. We use the fully-local (FLL) double counting correction in the calculation of both the bcc Fe and the Fe₁₆N₂ moments. Although this choice may seem strange in metallic systems, the around-mean-field (AMF) term opposes the formation of moments in general⁴⁸ and here produces moments $\sim 1\mu_B$ below the expected value in bcc Fe. It should be noted, however, that the choice of the double counting term in PBE + U is not unique and thus leaves an ambiguity in the calculated moments even if U and J were computed with a well-defined method..

E. Orbital Moment

In solids, the orbital moment is typically nearly quenched, but in some extreme cases, such as UN,⁴⁷ the orbital moment can be comparable to the spin moment. PBE calculations give an orbital moment per Fe of only $0.05 \mu_B$ in bcc Fe (Table IV), but this may be increased somewhat in Fe₁₆N₂. To explore this possibility, we calculated the orbital moment within PBE, PBE+orbital polarization correction (OPC),⁴⁹ PBE+U (using the cRPA parameters), and “one-shot” G₀W₀ using FPL0 (for the OPC calculation) and VASP (for the rest). Each method shows a small increase in orbital moment compared to bcc Fe, yielding about $0.1 - 0.2 \mu_B$ per Fe atom and an increase of $0.01 - 0.05 \mu_B$ over bcc Fe. This small increase cannot explain those results that claim average Fe moments in excess of $3 \mu_B$. Our PBE+U and G₀W₀ results predict average total (spin + orbital) moments of 2.88 and $2.63 \mu_B$, respectively.

IV. SUMMARY

We have examined the electronic and magnetic structure of α'' -Fe₁₆N₂ within PBE, PBE+U, HSE06, and GW. Within PBE, we find spin moments and hyperfine fields that agree with past results, and we do not find that any high-magnetization state arises as $\frac{c}{a}$ changes from the experimental value. We have provided effective Coulomb interaction parameters calculated via cRPA and have

Method	4d Site (μ_B)	4e Site (μ_B)	8h Site (μ_B)	Average (μ_B)	bcc Fe (μ_B)
PBE	0.06	0.06	0.05	0.06	0.05
PBE+U	0.20	0.16	0.16	0.17	0.12
PBE+OPC	0.09	0.11	0.10	0.10	0.09
G ₀ W ₀	0.06	0.06	0.05	0.06	0.05

TABLE IV. Calculated orbital moments in Fe₁₆N₂ within PBE, PBE+U, PBE+OPC, and G₀W₀. The orbital moment is increased by only 0.01 - 0.03 μ_B per Fe with respect to bcc Fe.

used them in our PBE+U calculations. We find that PBE+U and HSE06 gives average spin moments per Fe of 2.71 and 2.86 μ_B but also greatly overestimate the moment of bcc Fe (experimentally about 2.2 μ_B). GW gives smaller moments, 2.57 - 2.70 μ_B per Fe, a slight increase over the PBE moment. G₀W₀, GW₀, and GW all overestimate the bcc Fe spin moment by different amounts despite their similar predictions for Fe₁₆N₂, with G₀W₀ giving the most reasonable bcc Fe moment due to its close dependence on the PBE result. In all cases, we find that the 4e and 8h sites have smaller moments than that on the 4d site.

We have also presented calculations of the orbital moment on the Fe sites obtained within PBE, PBE+OPC, PBE+U, and G₀W₀. We find that the orbital moment is not completely quenched and may add 0.1 - 0.2 μ_B to the average total moment per Fe, a small increase over bcc Fe.

In order to evaluate the varying results found above, one must understand the purposes of and approximations inherent in the methods presented. In addition to the shortcomings of the mean-field-like treatment of correlations within PBE+U, there are two notable avenues for error in this method: the need to choose the U and J parameters and the lack of *a priori* justification for the double-counting corrections. Dependence on the choice of interaction parameters is not a fundamental problem and can be alleviated as we have done here by computing them through some appropriate first-principles method. The choice between the FLL or AMF double-counting corrections, while straightforward when treating insula-

tors, can be less obvious in semi-localized magnetic systems, and furthermore no method exists for determining the exact form of the correction. The hybrid functional method's dependence on parameters is fundamental to the approach, although it is mitigated somewhat by the use of predetermined parameters such as in HSE06. However, these parameters were primarily chosen to produce reasonable band gaps and may need to be altered to properly treat metallic systems. In principle, the GW approximation should be the most accurate of those presented here. The G₀W₀ and GW₀ methods maintain good contact with the PBE results while incorporating first-order exchange and correlation effects. However, some care must still be taken; we have shown that the results do depend on which electrons are treated as valence and which are absorbed into the core pseudopotential. Lastly, we note the need for additional, repeatable experiments that probe the electronic structure of the material in order to provide a better basis for comparison with theory.

V. ACKNOWLEDGMENTS

H.S. and W.H.B. acknowledge the support of NSF MR-SEC Grant No. DMR-0213985 and the use of computing resources from the Alabama Supercomputer Center. M.R. would like to thank Joachim Wecker and Manfred Rührig for discussion. E.Ş, C.F and S.B. acknowledge the support of DFG through the Research Unit FOR-1346.

¹ K. H. Jack, Proc. R. Soc. A **208**, 200 (1951).

² T. K. Kim and M. Takahashi, Appl. Phys. Lett. **20**, 492 (1972).

³ Y. Sugita, K. Mitsuoka, M. Komuro, H. Hoshiya, Y. Kozono, and M. Hanazono, J. Appl. Phys. **70**, 5977 (1991).

⁴ Y. Sugita, H. Takahashi, M. Komuro, K. Mitsuoka, and A. Sakuma, J. Appl. Phys. **76**, 6637 (1994).

⁵ A. Kano, N. S. Kazama, H. Fujimori, and T. Takahashi, J. Appl. Phys. **53**, 8332 (1982).

⁶ K. Nakajima and S. Okamoto, Appl. Phys. Lett. **56**, 92 (1990).

⁷ M. Takahashi, H. Shoji, H. Takahashi, T. Wakiyama, M. Kinoshita, and W. Ohta, IEEE Trans. Magn. **29**, 3040 (1993).

⁸ M. Takahashi, H. Takahashi, H. Nashi, H. Shoji, T. Wakiyama, and M. Kuwabara, J. Appl. Phys. **79**, 5564 (1996).

⁹ R. Coehoorn, G. H. O. Daalderop, and H. J. F. Jansen, Phys. Rev. B **48**, 3830 (1993).

¹⁰ J. M. D. Coey, J. Appl. Phys. **76**, 6632 (1994).

¹¹ A. Sakuma, J. Magn. Magn. Mater. **102**, 127 (1991); A. Sakuma, J. Phys. Soc. Jpn. **60**, 2007 (1991); A. Sakuma, J. Phys. Soc. Jpn. **61**, 223 (1992).

¹² S. Ishida and K. Kitawatase, J. Mag. Magn. Mat. **104-107**, 1933 (1992).

¹³ S. Ishida, K. Kitawatase, S. Fujii, and S. Asano, J. Phys. Condens. Matter **4**, 765 (1992).

¹⁴ B. I. Min, Phys. Rev. B **46**, 8232 (1992).

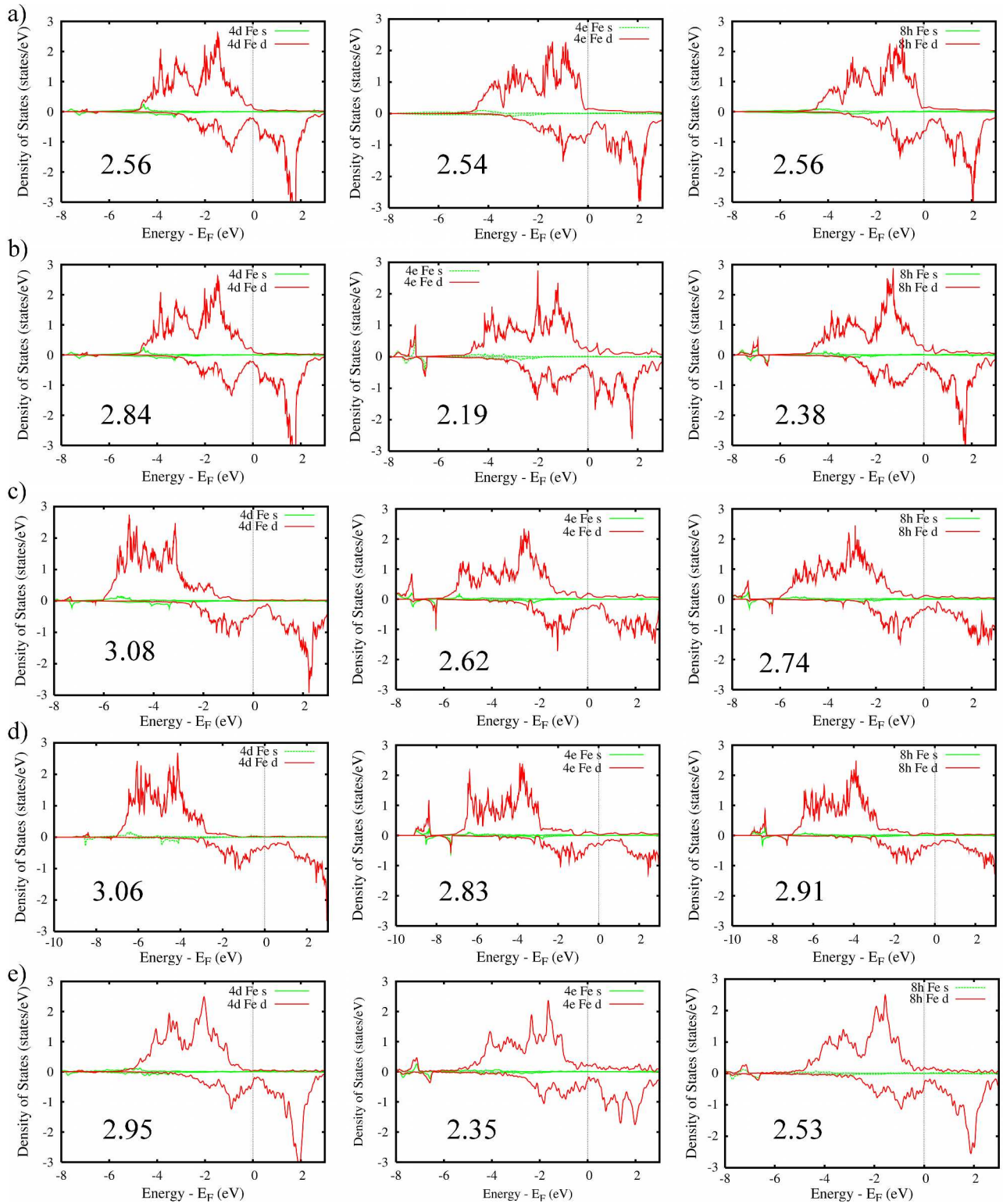


FIG. 3. (color online) *s* and *d* Partial density of states and spin moments (in μ_B) for the 4*d*, 4*e*, and 8*h* Fe sites (left, middle and right columns) for a) a fictitious Fe_{16}N_0 structure (within PBE) in which the Fe atoms retain their α'' positions. Here, we see that the majority channel is already nearly fully occupied due to the volume expansion induced by the N atoms. (b) PBE pDOS showing the effect of Fe – N hybridization: increasing the moment of the second-neighbor 4*d* site at the expense of the 4*e* and 8*h* sites. (c-e) PBE+U, HSE06, and GW_0 , respectively (the reader should note the difference in the scale of the *x* axis in the HSE plots): PBE+U and HSE06 each give large moments at each site, but predict an average moment only slightly larger than in bcc Fe (for which they also give very large moments). The pDOS for all VASP-GW methods considered in the text are in qualitative agreement with those displayed.

- ¹⁵ W. Y. Lai, Q. Q. Zheng, and W. Y. Hu, *J. Phys. Cond. Mat.* **6**, L259 (1994).
- ¹⁶ N. Ji, L. F. Allard, E. Lara-Curzio, and J.-P. Wang, *Appl. Phys. Lett.* **98**, 092506 (2011).
- ¹⁷ N. Ji, X. Liu, and J.-P. Wang, *New Journal of Physics* **12**, 063032 (2010).
- ¹⁸ V. I. Anisimov, J. Zaanen, and O.K. Andersen *Phys. Rev. B* **44**, 943 (1991).
- ¹⁹ J.-P. Wang, N. Ji, X. Liu, Y. Xu, C. Sánchez-Hanke, Y. Wu, F. M. F. de Groot, L. F. Allard, and E. Lara-Curzio, *IEEE Trans. Magn.* **48**, 1710 (2012).
- ²⁰ J. Heyd, G. E. Scuseria, and M. Ernzerhof, *J. Chem. Phys.* **124**, 219906 (2006).
- ²¹ L. Hedin, *Phys. Rev.* **139**, A796 (1965).
- ²² G. Kresse and J. Furthmüller, *Comput. Mater. Sci.* **6**, 15 (1996).
- ²³ F. Aryasetiawan, M. Imada, A. Georges, G. Kotliar, S. Biermann, and A. I. Lichtenstein, *Phys. Rev. B* **70**, 195104 (2004); F. Aryasetiawan, K. Karlsson, O. Jepsen, and U. Schönberger, *Phys. Rev. B* **74**, 125106 (2006); T. Miyake, F. Aryasetiawan, and M. Imada *Phys. Rev. B* **80**, 155134 (2009); B-C. Shih, Y. Zhang, W. Zhang, and P. Zhang, *Phys. Rev. B* **85**, 045132 (2012); T. O. Wehling, E. Şaşıoğlu, C. Friedrich, A. I. Lichtenstein, M. I. Katsnelson, and S. Blügel, *Phys. Rev. Lett.* **106**, 236805 (2011).
- ²⁴ E. Şaşıoğlu, A. Schindlmayr, C. Friedrich, F. Freimuth and S. Blügel, *Phys. Rev. B.* **81**, 054434 (2010).
- ²⁵ E. Şaşıoğlu, C. Friedrich, and S. Blügel, *Phys. Rev. B* **83**, 121101(R) (2011).
- ²⁶ C. Friedrich, S. Blügel and A. Schindlmayr, *Phys. Rev. B.* **81**, 125102 (2010).
- ²⁷ <http://www.flapw.de>
- ²⁸ J. P. Perdew, K. Burke, and M. Ernzerhof, *Phys. Rev. Lett.* **77**, 3865 (1996).
- ²⁹ L. Severin and M. Richter and L. Steinbeck, *Phys. Rev. B* **55**, 9211 (1997).
- ³⁰ K. Koepernik and H. Eschrig, *Phys. Rev. B* **59**, 1743 (1999), <http://www.fplo.de>.
- ³¹ M. Battocletti and H. Ebert and H. Akai, *Phys. Rev. B* **53**, 9776 (1996).
- ³² P. E. Blöchl, *Phys. Rev. B* **50**, 17953 (1994).
- ³³ G. Kresse and D. Joubert, *Phys. Rev. B* **59**, 1758 (1999).
- ³⁴ N. Marzari and D. Vanderbilt, *Phys. Rev. B* **56**, 12847 (1997).
- ³⁵ F. Freimuth, Y. Mokrousov, D. Wortmann, S. Heinze, and S. Blügel, *Phys. Rev. B* **78**, 035120 (2008).
- ³⁶ A. A. Mostofi, J. R. Yates, Y.-S. Lee, I. Souza, D. Vanderbilt, and N. Marzari, *Comput. Phys. Commun.* **178**, 685 (2008).
- ³⁷ C. Friedrich, A. Schindlmayr, and S. Blügel, *Comp. Phys. Comm.* **180**, 347 (2009).
- ³⁸ T. Moriya, Y. Sumitomo, H. Ino, and F. E. Fujita, *J. Phys. Soc. Jpn.* **35**, 1378 (1973).
- ³⁹ C. Ortiz, G. Dumpich, A. H. Morrish, *Appl. Phys. Lett.* **65**, 2737 (1994).
- ⁴⁰ S. Okamoto, O. Kitakami, Y. Shimada, *J. Mag. Magn. Mat.* **208**, 102 (2000).
- ⁴¹ K. Nakajima, T. Yamashita, M. Takata, and S. Okamoto, *J. Appl. Phys.* **70**, 6033 (1991).
- ⁴² J M D. Coey, K. O'Donnell, Q. Qi, E. Touchais, and J. H. Jack, *J. Phys. Cond. Mat.* **6**, L23 (1994).
- ⁴³ V. L. Moruzzi, P. M. Marcus, K. Schwarz, and P. Mohn, *Phys. Rev. B* **34**, 1784 (1986).
- ⁴⁴ M. van Schilfgaarde, T. Kotani, and S. Faleev, *Phys. Rev. Lett.* **96**, 226402 (2006).
- ⁴⁵ S. V. Faleev, M. van Schilfgaarde, and T. Kotani, *Phys. Rev. Lett.* **93**, 126406 (2004).
- ⁴⁶ Y.-R. Jang and B. D. Yu, *J. Mag.* **16**, 201 (2011).
- ⁴⁷ M. S. S. Brooks and P. J. Kelly, *Phys. Rev. Lett.* **51**, 1708 (1983).
- ⁴⁸ E. R. Ylvisaker, W. E. Pickett, and K. Koepernik, *Phys. Rev. B* **79**, 035103 (2009).
- ⁴⁹ L. Nordström, M. S. S. Brooks, and B. Johansson, *J. Phys.: Cond. Mat.* **4**, 3261 (1992).